BEACH MORPHODYNAMICS AND SEDIMENT TRANSPORT AT TIBJAK BEACH, CANADIAN BEAUFORT SEA COAST

Arnaud Héquette, Kimberley A. Jenner and Philip R. Hill

Hill Geoscience Research, Suite 220, 70 Neptune Crescent,

Dartmouth, N.S., B2Y 4M9, Canada.

TABLE OF CONTENTS

Abstract

Waves and currents were measured every three hours between August 27 and September 28, 1987, in 3.5 and 4.5 m of water depth, seaward of Tibjak Beach on the Beaufort Sea coast. During this period, five significant wind events from the west and northwest resulted in the generation of onshore-directed waves of relatively high amplitude (significant breaker height up to 1.4 m and significant period in excess of 8 s), associated with storm surges up to 0.85 m above mean water level. Visual estimates of breaking wave height, using video camera recordings from the beach, were accurate within ± 20% for 75% of the observations. The determination of breaker type using the surf-scaling parameter (ε), proved to be in good agreement with previous breaker type predictions. During the high-magnitude wave events, breakers were mainly of the spilling or plunging type. The type of breaking wave appears to be strongly controlled by water level fluctuations and incident wave amplitude. Morphodynamic beach states were defined using beach and nearshore topographic and bathymetric data, visual estimations of breaker types, and values of ε for every three-hourly wave data set. The modal beach state was intermediate between transverse bar and ridge and runnel types, with the subaerial beach being strongly reflective and the outer surf zone highly dissipative.

The net potential longshore sediment transport along Tibjak Beach for the whole study period (calculated from the CERC and Queen's equations) was 2.6 to 6.9 X 10^3 m^3 directed to the northeast. Beach profile surveying suggest that the beach experienced erosion of approximately 18.2 X 10^3 m^3 from August 22 to September 5. For this shorter period, potential longshore transport ranged from 1.9 to 4.3 X 10^3 m^3 suggesting that seaward sediment transport was important.

During most storms, high velocity seaward-directed currents, with mean speeds up to 0.5 m s^{-1} occurred in response to storm waves approaching obliquely from south of the shore-normal direction. These currents are interpreted as intensified rip currents resulting from storm surge residual flows. It is proposed that shallow channels truncating megaripples, in 4 m water depths seaward of

Tibjak Beach, were formed by these high velocity seaward currents. Because medium to fine-grained sands prevail on the shoreface, a significant sediment transport load is probably moved down the shoreface by such currents during major events, thus contributing to offshore sediment dispersal.

INTRODUCTION

Beach changes and sediment transport processes in the coastal zone of the Canadian Beaufort Sea are important to both geologists and engineers. Geologists require a knowledge of coastal processes to understand the characteristics of marine transgression in the offshore stratigraphic record of the Beaufort Sea (BLASCO et al., in press), while engineers will require similar information for effective design of coastal structures related to oil and gas production.

Although the Canadian Beaufort Sea is covered by sea-ice during six to nine months of the year, waves and currents are the dominant processes driving sediment transport in shallow nearshore and coastal waters (HARPER and PENLAND, 1982). Longshore sediment transport has been estimated at several sites along the Beaufort Sea coast by PINCHIN et al. (1985), based on a calculated nearshore wave climate derived from refraction analyses of hindcast deep-water waves. Prior to this study, only one set of measured wave data, from near King Point in 1985 (GILLIE, 1985) has been obtained. Given the paucity of existing directional nearshore wave data and the importance of such data to improving our understanding of sediment transport processes in the Beaufort Sea coastal zone, a detailed field program was carried out during the summer 1987 at Tibjak Beach on the Tuktoyaktuk Peninsula (Fig. 1). Wave and current meters were deployed in the nearshore zone (Fig. 2), and data were recorded from August 27 to September 17. During the same period, beach profiles, sediment samples, bathymetric profiles and sidescan sonar records were collected. In addition, video cameras recorded images of the beach and nearshore zone simultaneously with the current meters. In this paper, we present the results of this field program and discuss their implications for coastal and nearshore sediment transport processes at the site.

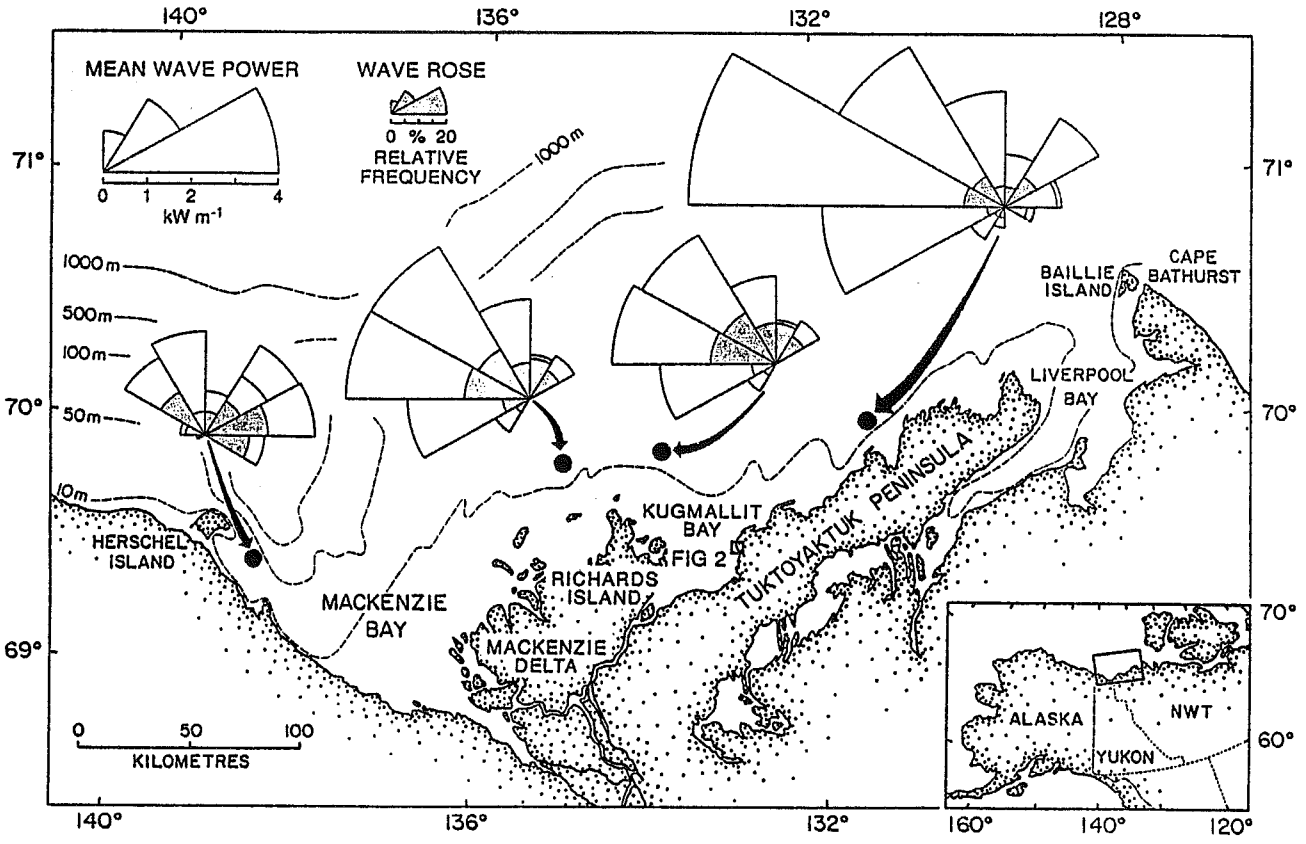

Figure 1. Location map of the Beaufort Sea and of the study area showing the directional frequency distribution of wave and of wave power (data from PINCHIN et al., 1985).

STUDY AREA

The study area is located along the Tuktoyaktuk Peninsula, on the eastern side of Kugmallit Bay (Fig. 1). The Tuktoyaktuk Peninsula forms a lowland of unconsolidated Pleistocene sands overlain in places by eolian or lacustrine sediments of Holocene age (RAMPTON, 1988). During the Holocene, relative sea level rose from approximately -70 m to its present level (HILL et al., 1985). Although the present rate of sea level change has not been clearly defined, geomorphological evidence suggests that a continuing rise of relative sea level (FORBES, 1980) probably contributes to retreat of the Tuktoyaktuk Peninsula coastline at an average rate of more than 1 m/a (HARPER et al., 1985; HEQUETTE and RUZ, in prep.).

The eastern Canadian Beaufort Shelf extends offshore to 70 m water depth and is characterized by a very gentle gradient in the range of 1: 2000. Muds dominate the central and outer shelf, while inshore of the 10 m isobath, fine sand generally predominates (VILKS et al., 1979). Surficial seabed sediments are underlain by a shoreward-thinning transgressive sand sheet generated by shoreface erosional retreat during Holocene sea level rise (HEQUETTE and HILL, 1989). The inner shelf and shoreface zones are dominated by the action of waves and currents. Winter sea-ice effectively limits wave energy for nine months of an average year and seaward of the 10 m isobath, sea-ice scouring of the seabed contributes to sediment erosion (HEQUETTE and BARNES, 1990). During the ice-free summer and fall, the pack-ice continues to influence wave energy through fetch limitation. Winds blow predominantly from the east, southeast and northwest quadrants during the open water season. However, most of the high energy waves originate from the northwest (Fig. 1) in response to storm winds and a longer fetch (HARPER and PENLAND, 1982). The Beaufort Sea is a moderate wave-energy environment with nearly 80% of deep-water waves less than 1 m in height. Tide-induced water level variations are small along the Canadian Beaufort Sea coast (mean tidal range: 0.3-0.5 m), but positive storm surges may raise water levels by as much as 2.4 m above mean sea level in the

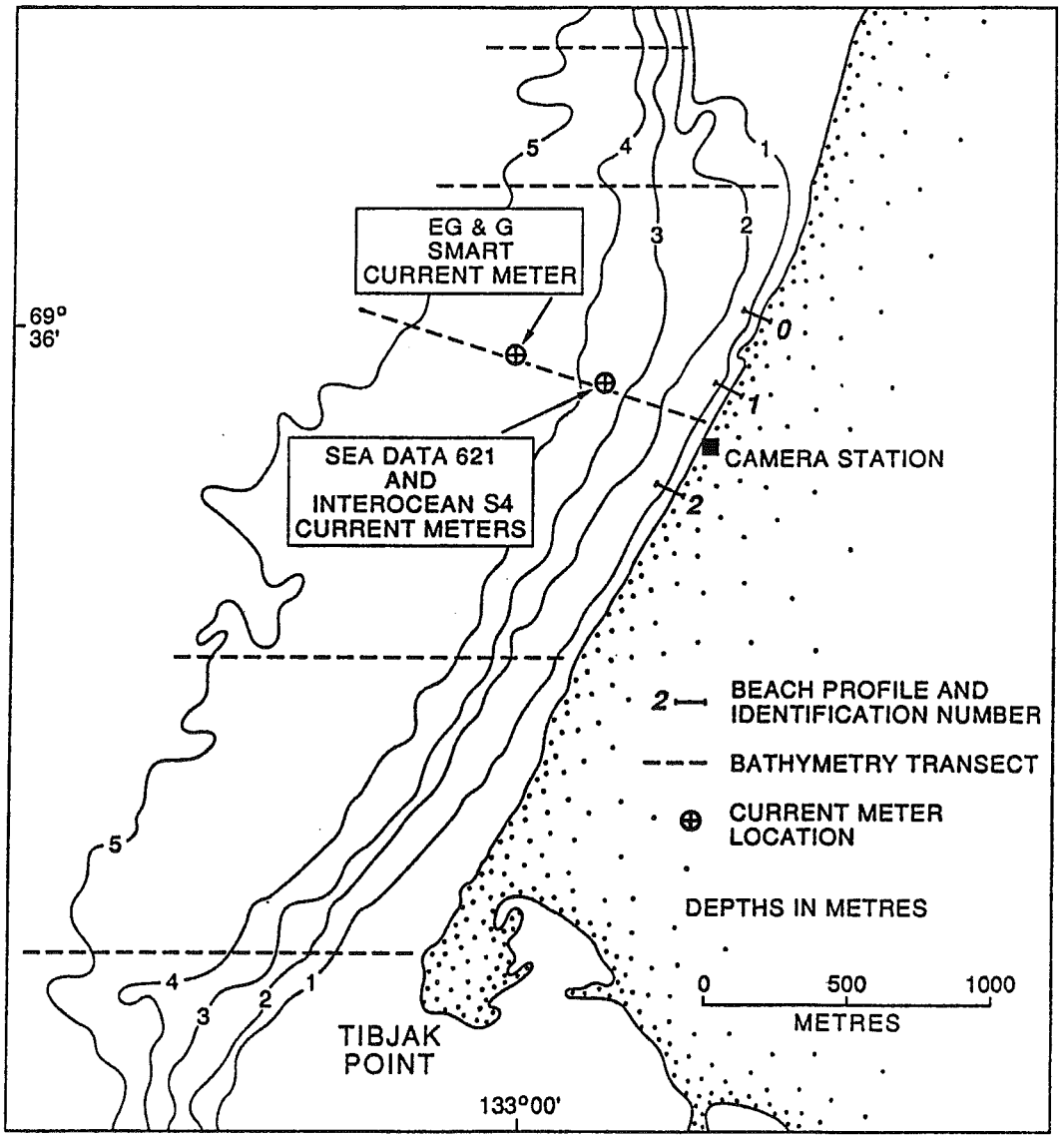

Figure 2. Map showing the Tibjak Beach study site and location of current meters, video camera and beach transects.

Kugmallit Bay area (HARPER et al., 1988).

Tibjak Beach is a 2.5 km long beach of medium-grained (Mz: 0.4 mm) well-sorted sands (Sorting index: 0.36 Ø). The beach is extended southward by Tibjak Point, a small sandy spit about 1.5 km long (Fig. 2). To the north, rapidly retreating sandy cliffs, up to 5 m high, supply sediment to the beach. The coastline faces WNW and is exposed to the dominant wave approach (Fig. 1). The backshore is characterised by small aeolian dunes with 1 to 2 m of relief. The general shape of the subaerial beach is linear (Fig. 3) although irregularly-spaced beach cusps may be visible at low tide. The nearshore zone exhibits a more complex morphology. A slightly oblique nearshore bar, approximately 40 cm high, extends towards the southwest just below low tide level along the central part of Tibjak Beach. At low tide, this bar may be truncated in places by low-relief channels. Towards the end of Tibjak Point, the nearshore area consists of a flat shallow platform with a system of multiple parallel bars. The northern part of Tibjak Beach is also characterised by a very flat nearshore zone (Fig. 2). The subaerial beach at the study site has a very steep slope (9° to 10°) which immediately flattens to about 1.5° in the subtidal zone to 1 m below Hydrographic Chart Datum and to 0.6° between the 1 m and 4 m isobaths. Bottom sediments across the shoreface are generally sandy (0.2-0.35 mm), and the upper metre typically consists of fine to coarse sand with occasional gravel-size clasts, commonly interbedded with silty sand or silt laminae (HEQUETTE and HILL, 1989).

METHODS

Beach and Nearshore Surveys

Beach profiles were measured in the central part of Tibjak Beach (Fig. 2). Three topographic transects were surveyed perpendicular to the shoreline using a theodolite and a tape-measure, with accuracy of ±5 cm in the vertical plane. All survey elevations in this paper have been reduced to Hydrographic Chart Datum, which corresponds to lowest normal tide, ≈ 0.4 m below mean sea level,

Figure 3. Oblique aerial photograph of Tibjak Beach (Tibjak Point in background).

using tide records at Tuktoyaktuk. The beach profiles were surveyed at the begining of the field program during calm conditions and at a later time, after storm conditions, in order to measure beach slope variations and to estimate beach volume changes. The bench mark for each profile is located in the backshore dunes, at elevations ranging from 3 to 4 m. They extend seaward in the subtidal zone to water depths of about 0.15 m below datum. Sediment samples were collected at the same time along the transects where textural variations occurred.

Five bathymetric lines were surveyed perpendicular to the coast from the R/V Karluk, using a 200 kHz echosounder with ±10 cm precision. A skiff equipped with an echosounder was used to survey each line up to the beach. Acoustic soundings were calibrated with lead line measurements between 2 and 7 m water depths. Sidescan sonar records were obtained using a Klein 500 kHz system and bottom sediment samples were collected with a Van Veen grab-sampler.

Wave and Current Data

Oceanographic instruments were deployed from August 27 to September 17 along a shore-normal transect (Fig. 2). A Seadata model 621 wave and current meter and an InterOcean model S4 current meter, spaced approximately 50 m apart, were deployed in 3.5 m water depth, approximately 400 m from the beach. An EG & G Smart Acoustic Current Meter was deployed on a separate mooring, in 4.5 m of water and 700 m from the beach.

All three instruments are true vector averaging current meters, having no moving parts which makes them well suited for measuring currents in the presence of large wave orbital velocities. Directional wave and current measurements were obtained from the Sea Data 621 instrument, which consists of a two-axis electromagnetic current meter and a strain gauge pressure transducer. The instrument, located 1.1 m above the seabed, was programmed to burst sample at 1 Hz, for 1024 consecutive seconds (17.07 minutes burst record duration), every three hours. The InterOcean S4, located 1.0 m above the seabed, recorded three-minute averages of velocity components every fifteen

minutes, with pressure, conductivity and compass heading once each hour. The EG & G Smart was located 1.0 m above the seabed and in this case, current meter, velocity and direction components were averaged and recorded at 10 minute intervals. Additional detailed technical specifications concerning these current meters may be found in FISSEL and BYRNE (1988).

In this paper, we present a detailed analysis of the directional wave and current measurements from the Sea Data model 621 meter. The current data from the two other instruments were used to compare the mean current distribution at the same water depth and in 4.5 m of water. Individual bursts from the Sea Data 621 data have been subject to spectral wave analysis for computation of appropriate wave parameters. These analyses yielded values of maximum amplitude of velocity fluctuations (which essentially corresponds to wave orbital velocity), mean wave direction, significant wave height (H_s), and peak wave period (T_p). In addition, mean current velocity and direction, and pressure have been computed as the mean of each three-hourly burst. Pressure is given in decibars (dbars) and in this case, because salinities in the area were low over the study period, can be considered equal to water depth. Changes in mean pressure at Tibjak Beach are consistent with water level variations recorded at Tuktoyaktuk (Fig. 4), and a simple linear regression analysis between these two data sets showed a fairly strong correlation ($r = 0.89$). Slight differences were observed between the two data sets, believed to be essentially due to local water level changes induced by site-specific tide, wind and (or) surge conditions, so the pressure measurements probably reflect more acurately the actual water level variations at the study site.

Video Monitoring

A timer-controlled video camera was positioned on the coastline during the period of wave and current measurements, to monitor changes in beach and oceanographic conditions. The camera was mounted on a 4 m high aluminum platform, near the edge of a low cliff ($\approx$ 2 m high) in the middle part of the beach (Fig. 2) was directed offshore to image the foreshore, breaker and surf zones. Poles of 2

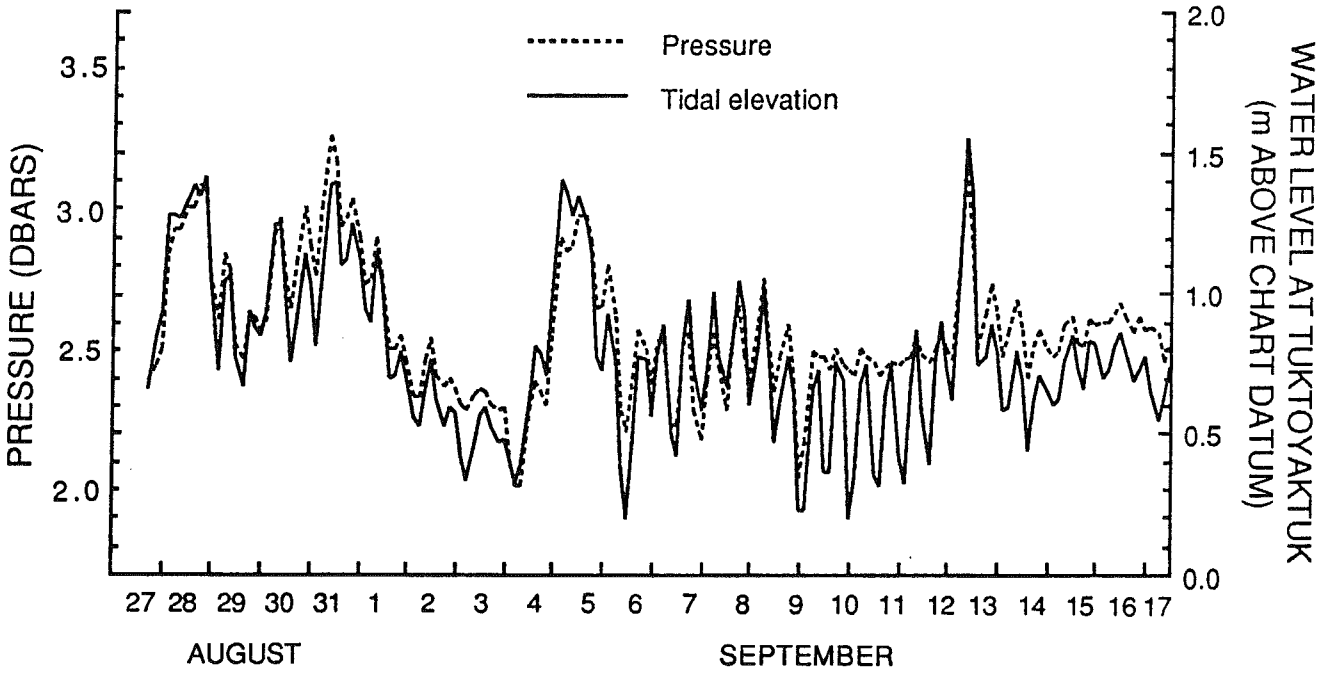

Figure 4. Time-series plot of pressure measurements at Tibjak Beach and of water levels recorded at Tuktoyaktuk.

m height were installed in the upper beach area to provide a scale on the video records. The camera was activated for a two minute period every 3 hours, simultaneously with the current meters. The camera recorded images of the beach and nearshore for the entire period of wave and current measurements except for the period September 3 to 8 due to power failure. Video records were used to estimate wave breaker height, define breaking type and make observations on water level fluctuations and beach morphology changes.

Longshore Sediment Transport Calculations

Longshore sediment transport was estimated using two bulk energy models. This type of model attempts to relate alongshore sediment transport rate to the wave energy flux or a related parameter such as wave energy density or the alongshore component of wave power. Two littoral transport rate formulae have been used to give a range of longshore sand transport estimates. One is the CERC formula (Coastal Engineering Research Center, 1977):

$$I_l = KP_l \qquad (1)$$

where I_l is the immersed weight longshore sediment transport rate, K is a dimensionless proportionality coefficient and P_l is the longshore component of wave energy flux in the breaking zone, defined as

$$P_l = 1/16\ \rho g\ H_{sb}^2\ n_b\ C_b \sin 2\alpha_b \qquad (2)$$

where ρ is the density of sea water, g is the acceleration of gravity, H_s is the significant wave height, n is the ratio of wave group velocity to phase velocity (and is virtualy equal to 1 at breakpoint), C is the wave phase velocity, α is the angle formed by the wave crest and the shoreline, and the subscript "b" refers to breaking wave conditions.

The immersed weight longshore sediment transport rate is related to the volume transport rate

(Q_l) through

$$I_l = (\rho_s - \rho)\ ga'Q_l \qquad (3)$$

(INMAN and BAGNOLD, 1963), where ρ_s is the sediment density, and a' is a porosity factor for the immersed weight of sand. Using Equation (1) and the above relationship defined by Equation (3), the longshore sediment transport rate may be expressed in terms of volume ($m^3\ s^{-1}$) as

$$Q_l = KP_l/\ (\rho_s - \rho)\ ga' \qquad (4)$$

From a series of field experiments, KOMAR and INMAN (1970) were able to suggest that the dimensionless coefficient K = 0.77, when the root-mean-square wave height (H_{rms}) is used to calculate P_l. In this study, H_s was used as the representative wave, and the value of P_l therefore halved, as the wave energy calculated from the significant wave height has been determined to be twice that obtained with the root-mean-square wave height (LONGUET- HIGGINS, 1952).

Recent evaluations of the relationship defined by KOMAR and INMAN (1970) show that the value of the dimensionless coefficient K generally averages 0.8 for modestly sloping beaches but that K may vary from about 0.5 to 1.5 depending on the beach slope, grain size and breaker type (e.g., BRUNO et al., 1980; WHITE and INMAN, 1989). In a recent synthesis of both empirical and experimental data, KAMPHUIS et al. (1986) redefined the coefficient K in terms of sediment size and beach slope to include their effect on the rate of energy dissipation in the surf zone. They developed an energy-related longshore sediment transport formula (known as the Queen's formula), based on extensive laboratory tests and on a broad set of field data:

$$Q'_l = 1.28\ (ß\ H_{sb}^{7/2}/D)\ \sin 2\alpha b \qquad (5)$$

where Q'_l is the dry mass longshore sediment transport rate expressed in $kg\ s^{-1}$, ß is the average slope of the beach/surf zone, i.e the breaking depth (d_b) divided by the distance from the still water line to the breaker (λ), H_{sb} is the significant breaker height, and D is the sediment diameter. Comparison with

field data indicated the validity of Equation (5), particularly with respect to changes in beach slope (KAMPHUIS et al. 1986). The mass transport rates were then converted to volumetric rates assuming a sand density of 2.65×10^3 kg m^{-3}.

Wave Refraction Analysis

Wave refraction analysis was carried out to determine wave breaker height and the wave crest breaking angle (α_b). A version of WAVENRG, (MAY, 1974) which traces wave changes along orthogonals, based on Airy wave theory, was used for the analysis. This software provides a simulation of both wave refraction patterns and breaking wave conditions. The computer simulation consists of forward tracking of wave orthogonals from a specified depth across a depth-matrix representation of the seabed, given an initial wave height, period, and direction. Changes in wave height, length, direction, and maximum bottom orbital velocities are simultaneously calculated at specified iterations along each orthogonal. Waves are broken when the wave height equals 0.78 times the water depth ($H_b/d_b = 0.78$). A value of 0.78 is reasonable for most wave theories, and agrees well with field measurements on beaches with low gradients (McCOWAN, 1894; SVERDRUP and MUNK, 1946; HARDISTY and LAVER, 1989). More details on the wave equations and refraction procedure used in the refraction software may be found in MAY (1974).

In this study, the significant wave orthogonal for each burst record was refracted from 3.5 m water depth to the break point. Peak period (T_p) was converted to significant period (T_s) using Darbyshire's empirically derived relationship $T_p = 1.14\ T_s$ (KOMAR, 1976, p.92). A large scale bathymetric depth matrix was constructed from 5 m water depth to the shoreline using a 1985 Canadian Hydrographic Field Sheet at scale 1: 20 000 (FS WA 10168) and bathymetry records collected during the 1987 field program. The final output give the following wave statistics at break point: wave angle (α_b), water depth (d_b), wave phase velocity (C_b), ratio of wave group velocity to

phase velocity (n_b), significant wave height (H_{sb}), and the longshore component of wave energy flux (P_l).

RESULTS

Atmospheric and Oceanographic Conditions

In the summer of 1987, weak to moderate easterly wind conditions prevailed at Tuktoyaktuk, 15 km south of the study site, except for the period August 20 to September 14 when a sequence of west to northwesterly storms occurred. Winds having speeds in excess of 15 m s^{-1} were measured at Tuktoyaktuk on August 28 and on August 31, and events with speeds up to 12-13 m s^{-1} on August 30 and on September 5, 6, 8, 9 and 13. In all cases, the winds blew from the west or northwest, approximately normal to Tibjak Beach. The wind fetch exceeded 500 km on August 27, decreasing to approximately 400 km by September 10, due to the advection of pack ice by the west to northwesterly winds (FISSEL and BYRNE, 1988). Consequently, wind and ice conditions were favourable for the generation of high amplitude surface waves during the study period. Few measurements of deep-water waves are available for this period, but significant wave height in excess of 3 m were recorded on August 28 in 32.5 m water depth, 65 km northwest of Tibjak Beach (Marine Environmental Data Service, Department of Fisheries and Oceans, Ottawa).

From August 27 to September 17, the wave regime at Tibjak Beach was dominated by waves from the west and northwest directions (Fig. 5). More than 90% of the recorded waves had directions between 260 and 310°. Although more than 50% of the waves recorded during this period had a significant height at breaking of less than 0.2 m, breakers in excess of 0.5 m represent more than 30% of the total wave occurrence (Fig. 5). Several strong wind events from the WNW (on August 28, 30, 31, and September 5), resulted in waves with significant breaker heights of more than 1 m and significant period up to 8.6 sec (Fig. 6). Wave events of somewhat reduced magnitude also occurred

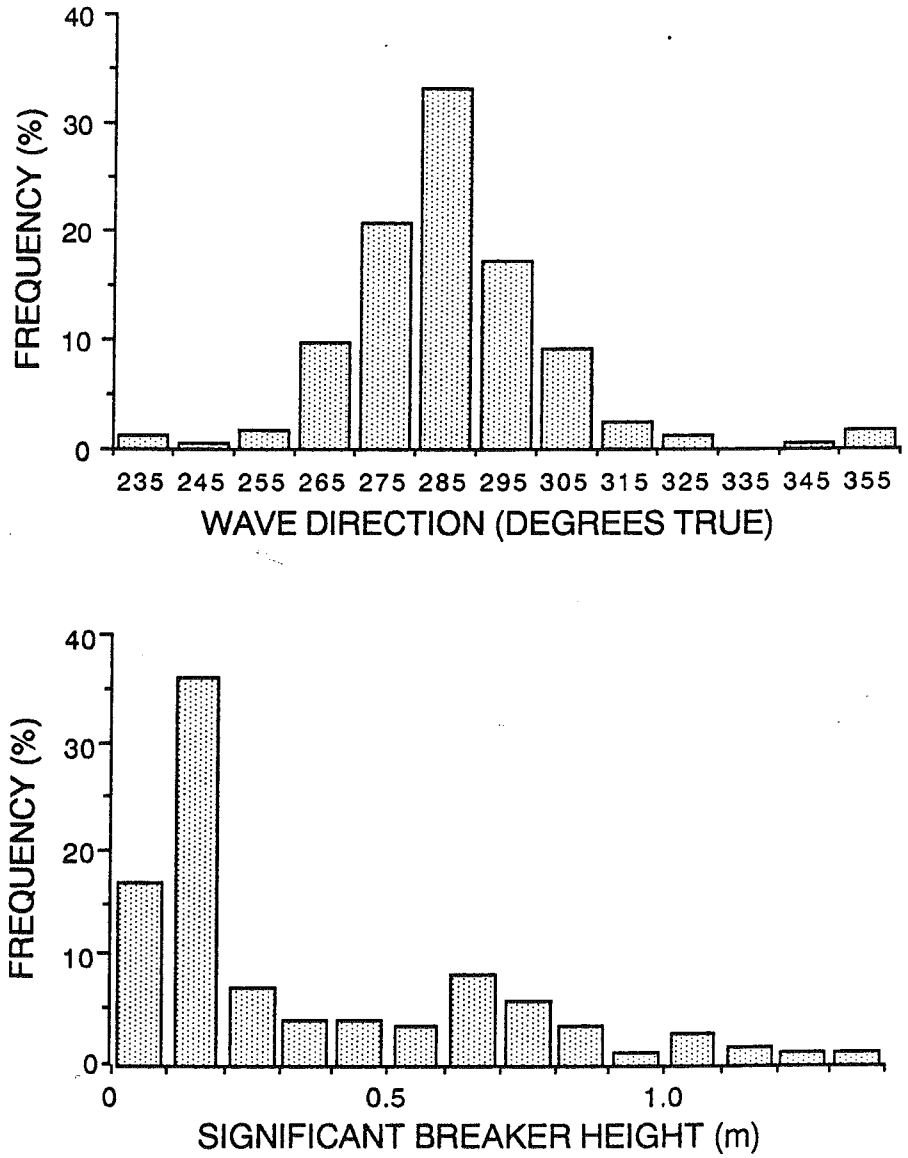

Figure 5. Distribution of wave direction (upper diagram) and significant wave height at breaking (lower diagram).

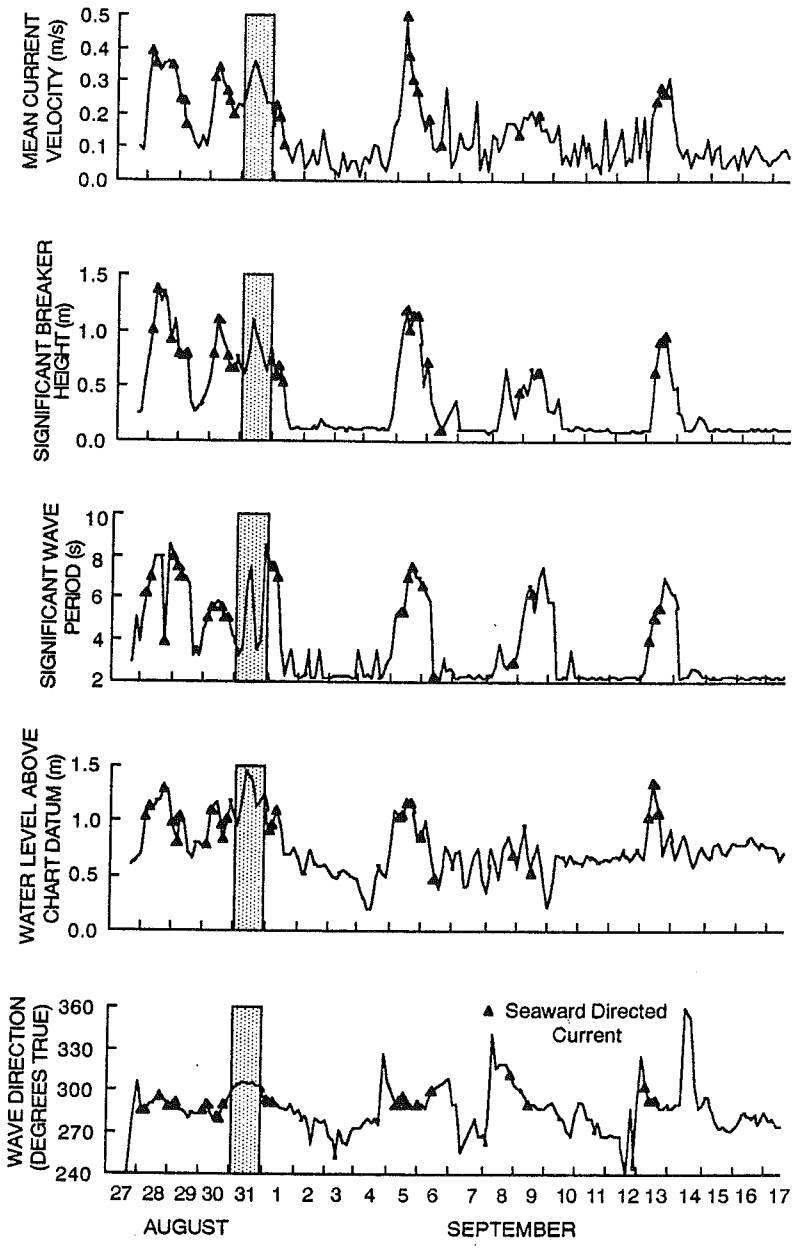

Figure 6. Time-series plot of mean current velocity, significant breaker height, significant wave period, mean water level, and wave direction obtained from Sea Data model 621 current meter data recorded 1.1 m from the bottom in water depth of 3.5 m, seaward of Tibjak Beach. Note that the significant breaker height represents computed values from significant wave height as recorded in 3.5 m water depth after refraction using a computer simulation; water depth is variable as it depends on the breaker height. The shaded area represents a storm event during which no offshore-directed currents occurred.

on September 8-9 and 13. High water levels (strorm surges up to 0.85 above mean sea level) and peak values in mean current velocities corresponded to each of these wave events (Fig. 6).

Visual Estimates of Breaking Wave Heights

Visual estimates of breaker heights from the video records were compared to significant breaker heights derived from the refraction analysis (Fig. 7). In general, the shoaling and refraction of the recorded waves to the breaker zone resulted in an increase in wave height of 10 to 30%. A reasonable estimate of breaker height was generally achieved from the video records, although some waves (especially the largest waves) were underestimated (Fig. 7). Despite this, about 75% of the visual estimates were accurate within ± 20% and for nearly 60% of the estimates, the error was less than 15%. From an extensive review of simultaneous visual estimates and measurements of breaking wave height, BALSILLIE and CARTER (1984) showed that observers are able to estimate breaking wave height with only 20% error,which is as good as the error expected with classical wave theories.

Morphodynamic Characteristics of Beach and Surf Zone

The video records were also used to distinguish the characteristics of breaking waves for different conditions. Surging, plunging, spilling breakers and transitional spilling to plunging breakers have been distinguished. GUZA and INMAN (1975) have shown that wave breaking characteristics and the degree of wave energy dissipation are dependant on the beach reflectivity which can be defined by the surf-scaling parameter:

$$\varepsilon = a_b \omega^2 / (g \tan 2 ß) \qquad (6)$$

where a_b is the breaker amplitude, ω is the wave radian frequency ($2\pi/T$; T = wave period), g is the acceleration of gravity, and ß is the beach/surf zone gradient. GUZA and BOWEN (1975) found that when $\varepsilon \leq 2.0\text{-}2.5$, low dissipation and strong reflection occur and breakers are of the surging type. As

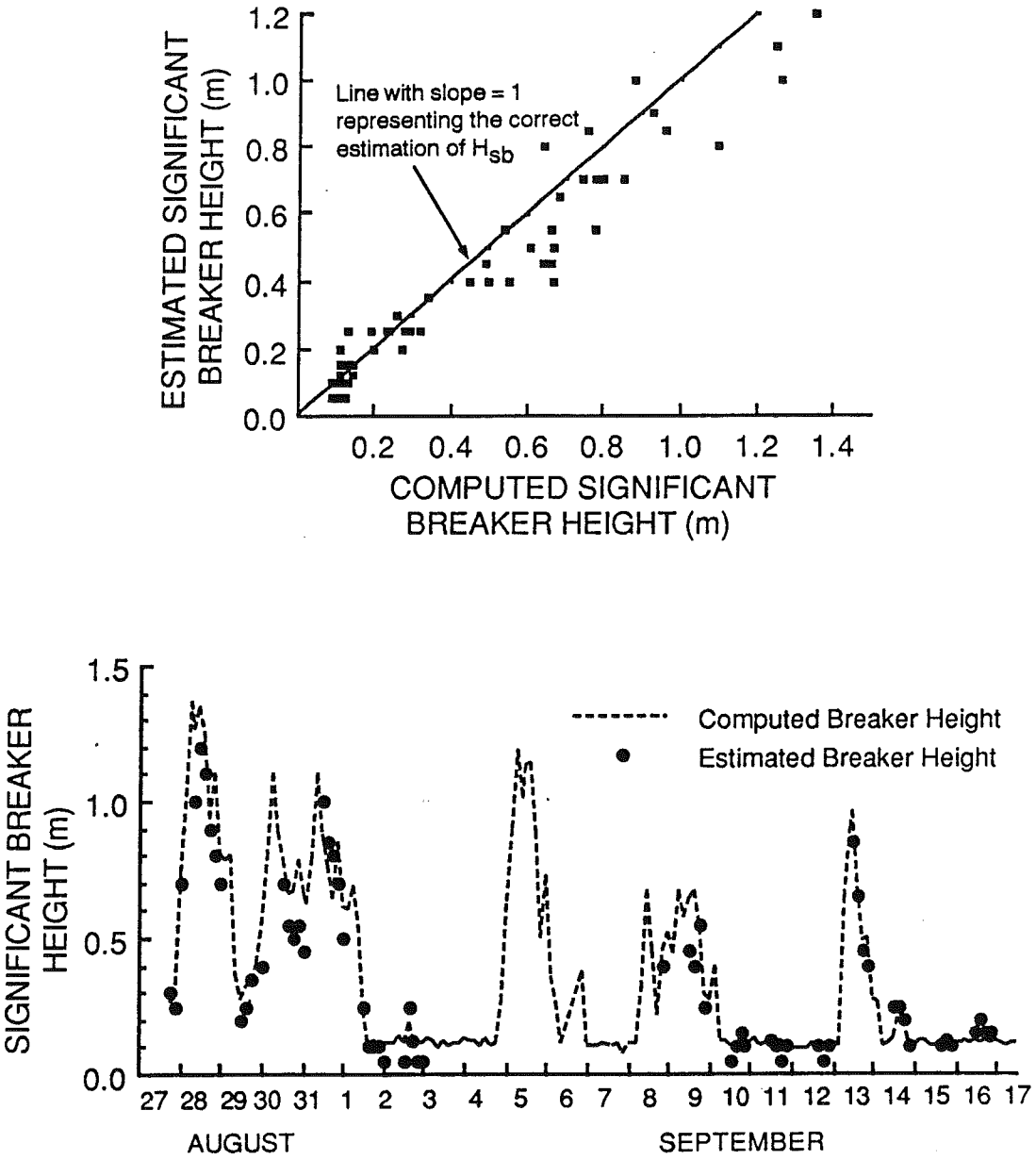

Figure 7. Comparison of visual estimates of wave breaker height using video records with computed breaker height after refraction of the waves recorded in 3.5 m water depth.

ε increases due to increasing wave steepness or to decreasing beach/surf zone slope, reflectivity decreases resulting in turbulent dissipation of incident wave energy. When $\varepsilon > 2.5$ waves begin to plunge causing a substantial increase in eddy viscosity, and when $\varepsilon > 30$ spilling breakers occur resulting in the dissipation of much of the wave energy before the waves reach the beach face.

In this study, the mean beach/surf zone gradient (ß) has been calculated by dividing the breaking depth (d_b) by the distance from the still water line to the breaker (λ). The available data for calculating ß included water level changes recorded at the study site, breaker depths obtained after refraction of the recorded waves, a shallow bathymetric profile (< 5 m water depth) obtained by acoustic sounding, and topographic data from beach and nearshore surveying (profile 1, Fig. 8). Because the bathymetry transect was recorded only once and the beach profile has been surveyed only twice during the period of the study, there is some approximation in the definition of ß as variations in the incident wave energy flux likely induce changes in the beach/surf zone slope. However, comparison of profile 1 at two different times showed little changes in the slope of the foreshore and inner surf zone (Fig. 8), and it was found that for similar wave conditions, the most significant variations in ß were induced by water level fluctuations (particularly during storm surges) rather than by actual changes of the beach profile.

Except for a relatively small number of waves, our field data agree reasonably well with the breaker type classification based on the surf-scaling parameter (Fig. 9). There are however some discrepancies between the limiting values of ε obtained in this study for differentiating breaking wave types and values proposed earlier for discriminating between breaker types (e.g. GALVIN, 1972; GUZA and BOWEN, 1975). From our observations at Tibjak Beach, waves cease to surge up at the beach and begin to plunge when $\varepsilon < 1.5$, and there is a transition from plunging to spilling breakers

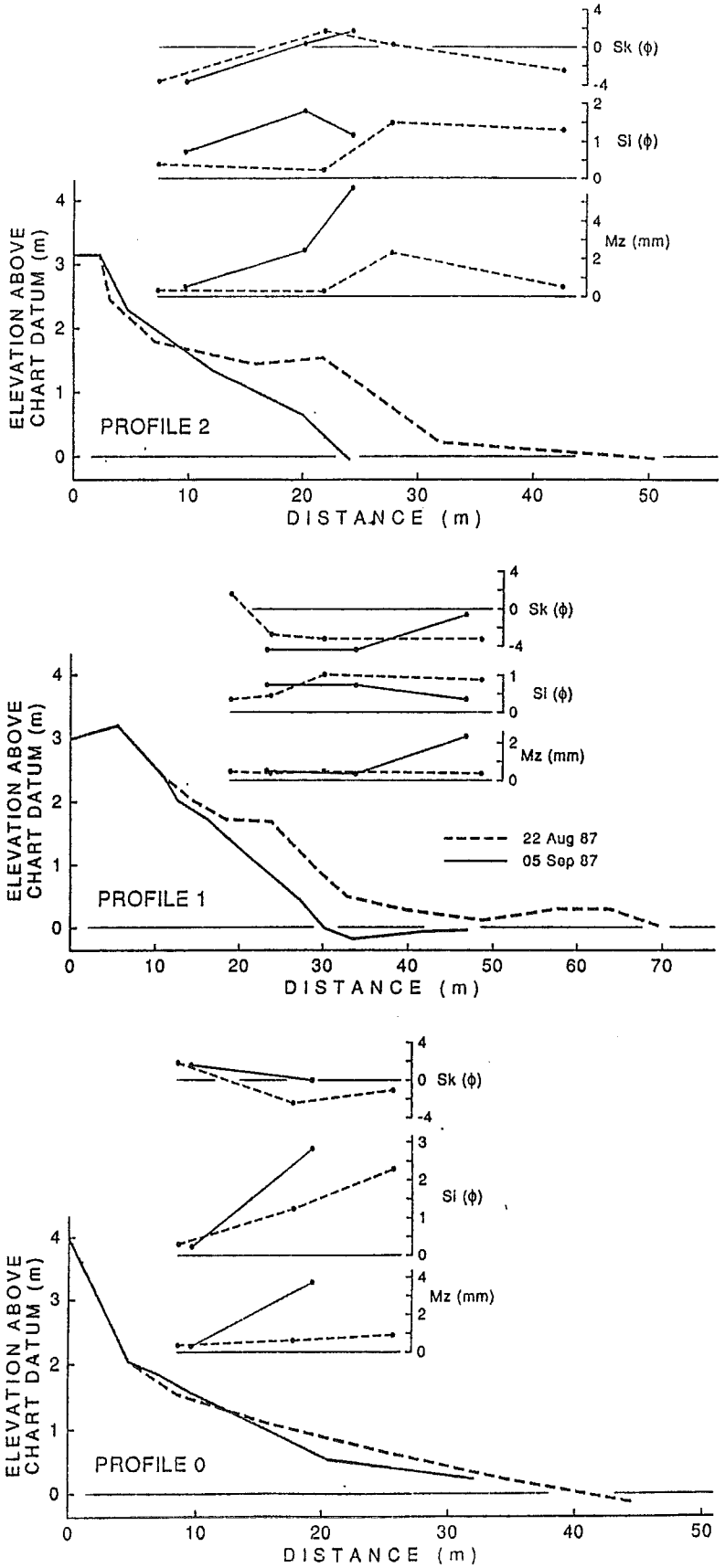

Figure 8.. Variations in beach profile and sediment texture at Tibjak Beach (see Fig. 2 for beach profiles location).

between $\varepsilon = 20$ to 35 (Fig. 9). Plunging breakers that fall on both sides of these limits, can be explained either by the difficulty in estimating the breaker type for small waves or by unsurveyed slope variations in the case of larger waves.

Except for the very small waves ($H_{sb} < 0.15$ m) which were generally breaking directly on the foreshore and the highest waves that were usually breaking in the outer surf zone, most of the plunging and plunging-spilling waves were breaking over the nearshore bar surveyed on August 22 (Profile 1, Fig. 8) or on its seaward slope.

The surf-scaling parameter may also be used to distinguish morphodynamic beach states, or domains, which are characterised by distinct morphological characteristics and wave-generated hydodynamic processes. According to the model developed by WRIGHT et al. (1979) and by WRIGHT and SHORT (1984), there are two extreme and opposite beach states, the fully dissipative and the highly reflective, separated by four intermediate states, each beach state being defined by specific morphologies associated with various breaking wave conditions. Reflective beach states are distinguished by values of $\varepsilon < 2.5$ and are characterised by linear steep beach slopes and low-amplitude waves breaking on or very close to the foreshore. The value of ε typically exceeds 20 on dissipative beaches, which are characterised by a flat shoaling slope and a wide surf zone. The dissipative state prevails in the presence of high steep waves and (or) fine-grained sediment. Between the two extremes are four intermediate states (longshore bar-trough, rythmic bars, transverse bars, and ridge-runnel/low tide terrace) possessing both dissipative and reflective elements.

As shown in Figure 9, the beach and surf zone at Tibjak Beach can be of the reflective, dissipative or intermediate type according to the surf-scaling parameter, depending on the wave conditions of the moment. As expected, reflective conditions are associated with low-amplitude waves and higher waves correspond to more dissipative conditions as they break farther offshore over the flat sloping bottom of the outer surf zone. Although the highest waves ($H_{sb} > 0.7$ m) tend to be of the

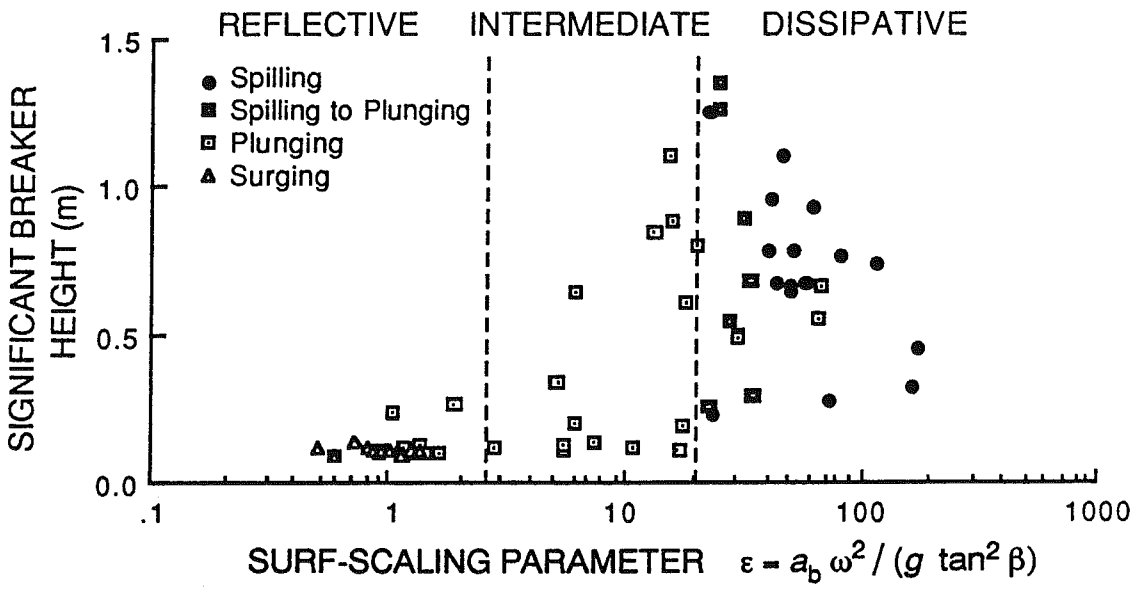

Figure 9. Relationship between breaker height (H_b) and the surf-scaling parameter (ε). Breaking wave types are visual estimations using video records. The limits between beach morphodynamic domains are taken from WRIGHT and SHORT (1984).

energy-dissipative spilling type, some small waves correspond to highly dissipative conditions with values of ε that may be in excess of 100 (Fig. 9). This is due to low water levels causing the waves to break relatively far from the beach which results in corresponding low ß values. Therefore, the beach and surf zone at Tibjak Beach posses several morphodynamic domains dominated by more or less reflective or dissipative conditions. The cross-shore extent of these domains varies mainly as a function of changes in wave height and water level. Generally speaking and for mean water level conditions, the reflective domain is confined to the subaerial beach and foreshore zone, the bar and trough system in the inner surf zone (Profile 1, Fig. 8) is characterised by variable and mixed reflective and dissipative conditions depending on the wave amplitude, and the outer flat shoaling surf zone is a highly dissipative domain. However, the entire beach and nearshore system is in equilibrium with the modal or prevailing hydrodynamic conditions and exhibits morphologies corresponding to such conditions. The combination of morphological characteristics and wave breaking types occurring at the study site reveals that this part of the beach and inshore system is representative of one of the intermediate beach states of WRIGHT and SHORT (1984) classification. It probably corresponds to a combination of the "transverse bar" and "ridge-runnel/low tide terrace" states as the beach and nearshore zone is characterised by an oblique bar close to shore and by low-tide cusp-like features, and because plunging and plunging-spilling breakers seem to be the most persistent breaker types whatever tide and offshore wave conditions are, which is characteristic of such beach states. Furthermore, most of these waves are breaking over the nearshore bar as mentioned previously, suggesting that they are responsible for the formation of the bar. Therefore, such waves (with breaker height between 0.4 and 0.7 m, and period ranging from 3 to 7.5 sec) probably represent modal wave conditions with which the Tibjak Beach system is in equilibrium.

Beach Changes and Longshore Sediment Transport

During the study period, significant morphological and sedimentological changes occurred on

the beach. Profiles surveyed on August 27, before the first significant wave event (August 28), showed a well developed berm at sites 1 and 2 and a planar foreshore at site 0 (Fig. 8). The action of high-amplitude waves combined with high water levels resulted in the erosion of this berm by September 5. Changes in beach grain-size were also noted between August 22 and September 5. Although the mean size of the subaerial beach sands remained constant at 0.4 mm, a greater proportion of gravel was present on the lower foreshore on September 5 (Fig. 8). The gravel is interpreted to be a lag deposit resulting from erosion and winnowing by storm waves.

Changes in beach volume between August 22 and September 5 were estimated from the cross-sectional area of eroded sediment on the beach profiles. A volume of 15.4 m^3 per metre of coastline was eroded at site 2, 13.2 $m^3\ m^{-1}$ at site 1, and 3.5 $m^3\ m^{-1}$ at site 0, giving a total of approximately 9.6 X 10^3 m^3 of sand for the length of beach between sites 2 and 0. Assuming that beach erosion wesward of profile 2 is similar to the erosion measured between profiles 1 and 2, a mean value of 14.3 $m^3\ m^{-1}$ was used to estimate changes in beach volume for the rest of the beach. These calculations gave a total volume of 18.2 X 10^3 m^3 of beach sand removed along Tibjak Beach, excluding the spit at Tibjak Point. Similar erosion may have occurred along the spit, but this was excluded in order to obtain a minimum volume of sediment eroded from the beach.

Potential longshore sediment transport was also estimated using the CERC and the Queen's formulae (Fig. 10). Sediment transport was directed northward during all major storms, except for one event on August 31 - September 1, when net longshore transport was to the south (Table 1). The greatest transport occurred during the August 28-29 storm (Fig. 10) with a potential northward transport of 3.5 x 10^3 m^3 corresponding to a 36 hour storm period (Table 1). During this storm, waves were breaking with a height of 1.2 to 1.3 m (H_{sb}) for at least 9 consecutive hours. The direction of littoral drift was sensitive to small changes in wave angle about the shore-normal direction (295°). The northward sediment transport events were generally induced by waves approaching from

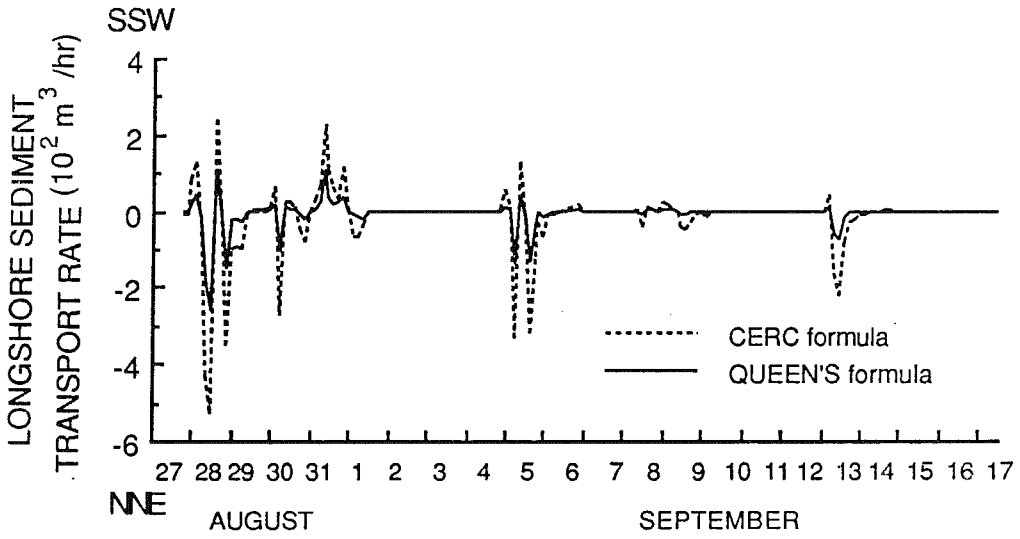

Figure 10. Time-series plot of potential longshore sediment transport rate at Tibjak Beach between 1987 August 27 and September 17 based on the CERC (SPM, 1977) and the Queen's (KAMPHUIS et al., 1986) formulae.

Date	Duration (hrs)	Average Wave Direction (^{0})	Net Longshore Sediment Transport (m^3) CERC Formula	Queen's Formula
28-29 August	36	285-295	-3580	-1565
29-30 August	33	285-290	- 670	- 295
31 Aug - 1 Sept	33	295-305	1460	650
4-5 September	36	290-300	-2130	- 865
8-9 September	42	285-315	- 365	- 56
13 September	24	290-300	-1510	- 515

Table 1. Net longshore sediment transport at Tibjak Beach for all significant wave events between 27 August and 17 September 1987. Calculations are based on the CERC (1977) and Queen's (Kamphuis et al., 1986) formulae. Alongshore transport to the southwest is taken as positive.

280° to 295°, but when the wave direction was greater than 295°, southward transport occurred.

For the entire period of the study, net longshore transport was estimated at 6.9 X 10^3 m^3 using the CERC formula and 2.6 X 10^3 m^3 using the Queen's formula, both directed to the north. These estimates are consistent with the surveyed profiles which show a decrease in beach erosion from north to south along the beach. The northward transport along Tibjak Beach during westerly storms probably results in the infilling of the small shallow embayment located to the north of the beach (Fig. 2). Southward sand transport is probably induced by waves from the northwest, north and northeast quadrants which represent a significant proportion of the total wave climate (Fig. 1).

The potential longshore transport for the period August 27 to September 5 was 1.9 X 10^3 m^3 and 4.3 X 10^3 m^3 to the north (Queen's and CERC formulae respectively). As relatively calm conditions prevailed between August 22 and August 27, beach changes and net transport can be considered negligible prior to the storm of August 28-29. The measured beach erosion between August 22 and September 5 (18.2 X 10^3 m^3) is higher than the calculated potential longshore sediment transport between August 27 and September 5, by as much as an order of magnitude. These results suggest that if the littoral transport formulae provide a reasonable approximation of the actual longshore transport, then a large proportion of the beach sand must have been transported seaward.

Coastal Currents

The greatest fluctuations in current velocities during the measurement period resulted from surface wave motions. Large wave orbital velocities were measured during each storm event from the west and northwest with peak values ranging from 0.65 to 1.3 m s^{-1} towards the shore (FISSEL and BYRNE, 1988). A significant increase in mean current velocities also occurred during storms (Fig. 6). At both measurement sites, in 3.5 and 4.5 m water depths, the directional distribution of mean currents was bimodal, setting in the longshore direction either to the NNE or SSW (Fig. 11).

A secondary component of current direction, perpendicular or slightly oblique to the shore, is

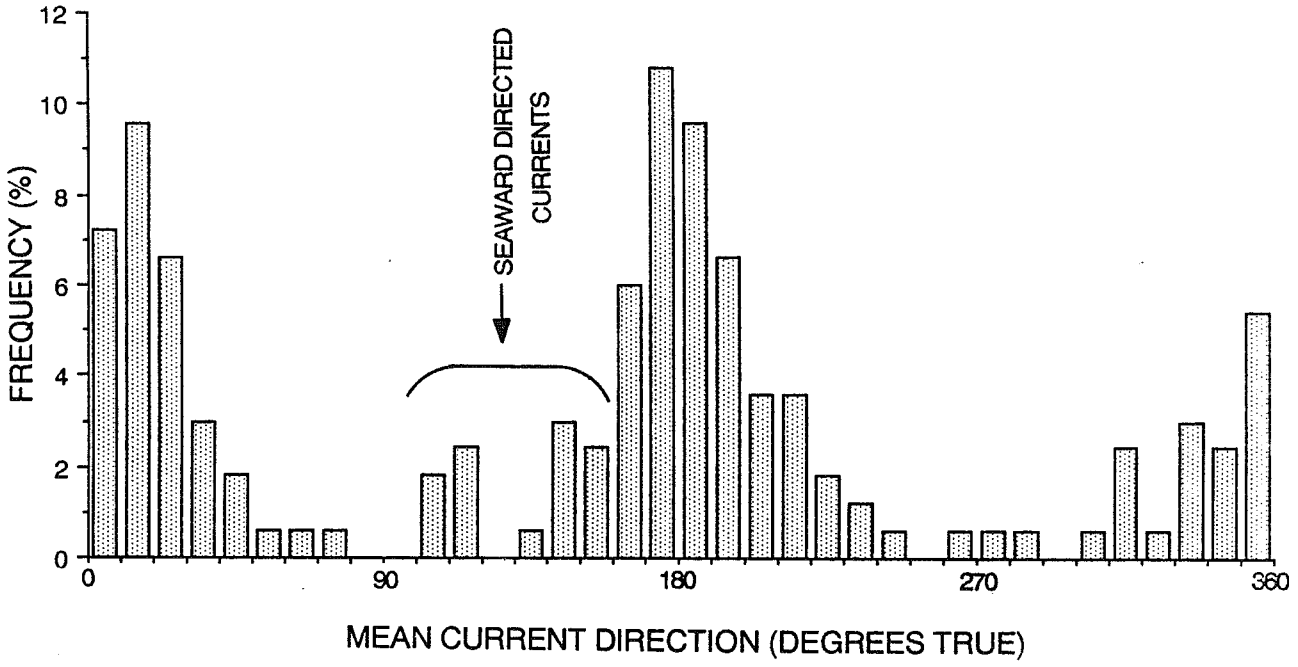

Figure 11. Directional distribution of mean currents as recorded by the Sea Data 621 instrument (water depth is 3.5 m).

also apparent from Figure 11. If currents less than 0.04 m s^{-1} are ignored, virtually all the seaward current events correspond to storm wave conditions and correspondingly high water levels (Fig. 6). However, during one storm, on August 31, breaker heights were in excess of 1m and mean water level was raised by approximately 0.8 m, but no seaward-directed currents were observed. Examination of wave approach directions strongly suggests that wave direction controlled the occurrence of these seaward-directed currents. During storms when strong seaward-directed currents were observed, waves approached from between 280° and 295° and net longshore transport was to the north. On August 31, when no seaward-directed currents were observed, waves approached from 305° and net longshore transport was to the south. Therefore, it seems that the seaward-directed currents correspond to a northerly wave set-up and periods of northward longshore transport.

The seaward-directed currents varied in duration from one event to another, but were generally persistent during each storm. On August 28-29, and September 1, 5 and 13, mean currents were directed offshore for periods of 6 to 9 consecutive hours, and during the August 30 storm, seaward-directed currents occurred almost continuously for 18 hours. During these events, current speeds were typically in the range of 0.25 to 0.35 m s^{-1} but a mean current velocity as high as 0.5 m s^{-1} was recorded during the September 5 storm.

The distribution of current direction from the two other instruments is consistent with the Sea Data 621 data showing a bimodal distribution, setting in the longshore direction, with a less-frequent seaward-directed component. However, current speeds were significantly lower at both measurement sites. At the InterOcean current meter, also in 3.5 m of water, the velocity of seaward-directed currents generally ranged from 0.10 to 0.20 m s^{-1}. Like the Sea Data 621 current meter, the strongest mean currents occurred on September 5, but had a magnitude of only 0.35 m s^{-1}. At the deeper site, in 4.5 m of water, the speed of the seaward-directed current was always less than 0.20 m s^{-1}, showing a marked seaward decrease in current intensity.

Two types of nearshore flow circulations can explain such seaward-directed currents: (i) rip

current cell circulation; or (ii) storm-induced bottom return flows. Several field experiments have shown that intermediate beach states are characterised by rip current circulation of variable intensity and that strong rip currents with speeds of the same order of magnitude as the breaking wave orbital velocities occur in association with intermediate transverse bar topographies (WRIGHT and SHORT, 1984). At Tibjak Beach, the beach and nearshore exhibit typical intermediate beach state morphology, with a discontinuous nearshore bar, consistent with rip current occurrence. In addition, values of ε during the seaward-directed current events were mostly ranging from 20 to 40 which correspond to intermediate to dissipative conditions, favouring development of rip current circulation. The lower current velocities recorded at the same water depth, only a few tens of metres from the Sea Data 621 instrument, suggest a laterally-restricted flow consistent with a rip current. However, the existence and distribution of rip current circulation patterns are often explained by subharmonic or infragravity edge waves (BOWEN and INMAN, 1969; KOMAR, 1976) having frequencies lower than the incident wave frequencies, but the analyses of wave spectra corresponding to seaward current events did not reveal evidence for such waves. Also, no sign of rip current activity was observed from either the surf zone or through the breaking wave train in the video records.

Seaward-directed currents may also be generated by near-bottom return flows induced by storm surges. It has been shown that onshore surficial water transport with coastal set-up, similar to the conditions observed during this study, may result in general downwelling and generation of a strong seaward-flowing current (NIEDERODA et al., 1984), possibly through a complex interaction with coast-parallel geostrophic jets (SWIFT et al., 1985). Time-series measurements of mean current velocities (Fig. 6) show that during each storm, seaward currents almost always began at the peak of current activity and continue to occur during a decreasing phase. This shows that seaward currents occur after the initial storm-induced increase in mean current velocity and could represent a residual flow, following release of the onshore stress (or coastal set-up) created by a storm surge. Such conditions can also intensify rip currents (SWIFT et al., 1985), so that seaward-directed currents on

the Tibjak Beach shoreface may result from a combination of storm-driven rip current circulation and near-bottom, surge-induced return flows.

Nearshore Bedforms

Side-scan sonar was used to survey the nearshore zone along Tibjak Beach on September 6, the day after a storm that resulted in the strongest seaward-directed currents. Several fields of megaripples, oriented almost parallel to the shore, were present in about 4 m water depth, close to the current meter sites and over a distance of at least 800 m to the southwest (Fig. 12). The megaripples have wavelengths of 0.7 - 0.8 m and show mainly sinuous crests. Bifurcating crestal patterns suggest a wave-induced origin for these bedforms (REINECK and SINGH, 1980). Neither the exact heights, nor asymmetry of these bedforms could be measured due to their scale and to distortion of the record by surface wave activity. They occur in narrow fields that are oriented nearly perpendicular to the beach and separated by less reflective areas (Fig. 12). The megaripples at the southern edge of the field are associated with positive relief up to 40 cm above the surrounding topography. Within the area of megaripples, the less reflective areas form shallow channel-like depressions 15 to 20 cm deep. The sharp boundaries of the less-reflective areas truncate the megaripples, suggesting that they formed after the megaripples.

The origin of nearshore bands of megaripples, in similar water depths and with similar configurations and orientations, has been tentatively attributed to rip currents (REIMNITZ et al., 1976) or to combined rip currents and subsequent wave action (MORANG and McMASTER, 1980). However, the megaripples described by these authors typically occur in depressions resembling channels, rather than on elevated areas as in the case of Tibjak Beach. Alternatively, FOX (in MORANG and McMASTER, 1980; p. 837) suggests that rip currents form plane beds, as they operate at the transition between upper and lower flow regimes. These plane beds may be reworked into megaripples by subsequent wave action.

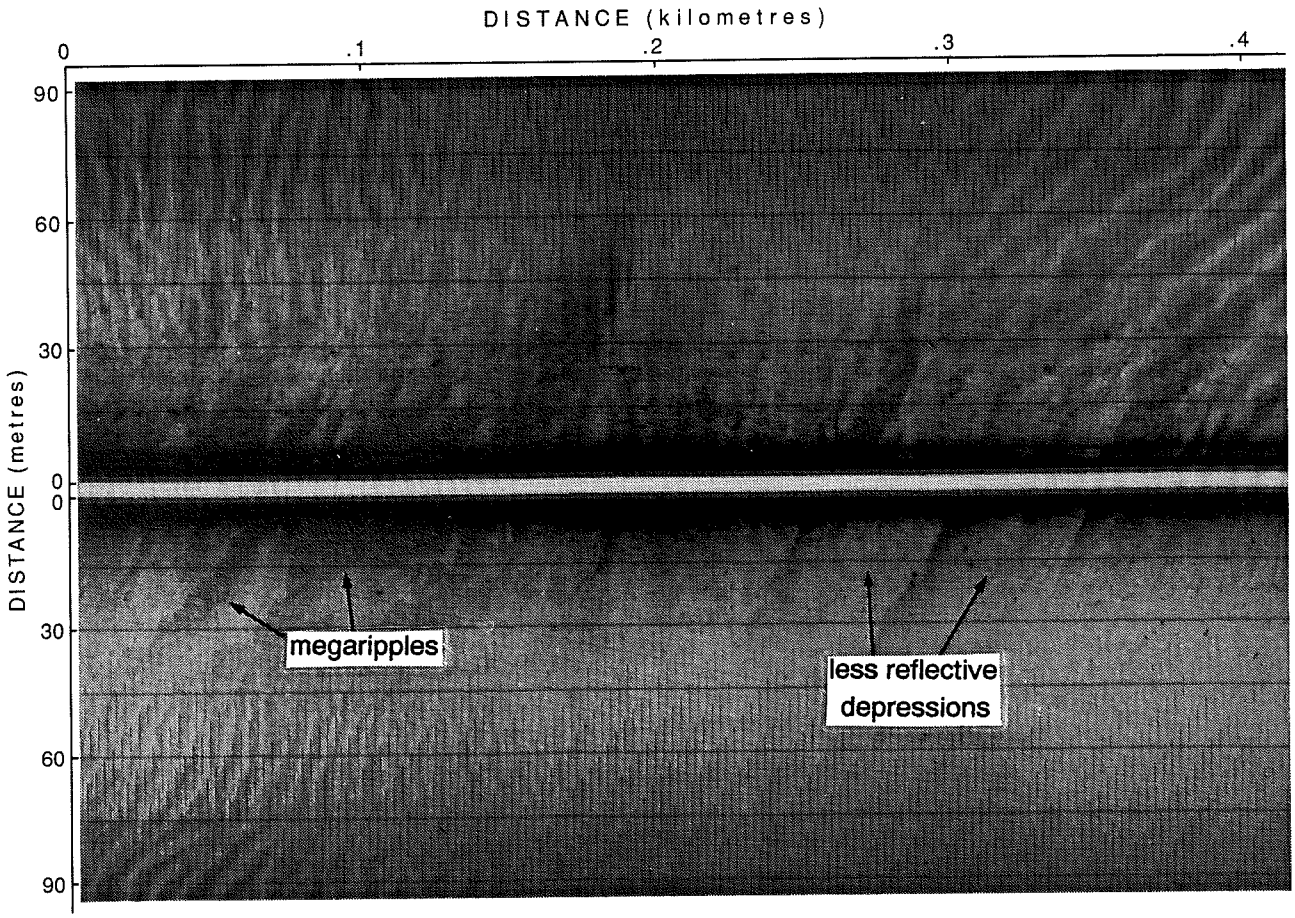

Figure 12. Sidescan sonar record showing bands of megaripples and flat shallow channel-like features perpendicular to the coast, 200 m southwest of the Sea Data 621 current meter, 6 September 1987. Shore side at bottom. Water depth along side-scan fish trackline is 4.0 m below chart datum.

We tentatively suggest that, at Tibjak Beach, the less reflective depressions may be the sites of channelized flows produced by rip currents. Although, the main body of a rip current flows in the upper part of the water column, the seaward flow of a rip current can extend from the surface to the bottom in water depths less than 5 m (COOK, 1970). Rip channels are known to occur even seaward of the breaker zone (SHEPARD et al., 1941). The megaripples at Tibjak Beach are interpreted to have been formed by incident wave-induced currents, possibly during the increasing phase of the September 5 storm. The megaripples were subsequently incised by seaward-flowing rip currents, which deposited the more homogeneous and non-reflective sand patches.

DISCUSSION

An important result of the Tibjak Beach study is the identification of two distinct sediment transport patterns that occur in response to moderate storm wave conditions. The first occurs under wave approach from directions to the north of shore normal (>295°) and is characterised by longshore transport towards the southern end of the beach. The second pattern occurs under wave approach from south of shore normal (<295°), and is characterised by a more complex circulation involving longshore transport towards the northern end of the beach combined with seaward-directed currents of either rip current or bottom return flow origin. While it is not clear why seaward-directed currents should occur under one condition and not the other, both conditions must occur relatively frequently, as wind and wave approach from both sectors is common (Fig. 1; Pinchin et al., 1985). There is morphological evidence for longshore transport in both directions. The flattening of the nearshore profile towards the north and infilling of the small embayment formed by the headland has resulted from northward longshore transport, whereas southward sediment transport has built the Tibjak Point spit.

The seaward-flowing currents are probably responsible for a significant part of the net sediment transport. Discrepancies between predicted lonshore sediment tarnsport potential and

observed sediment losses from the beach suggests a significant offshore transport of sediment. The seaward-directed currents are clearly strong enough to cause significant transport. According to laboratory experiments, a flow velocity of 0.5 m s^{-1} at 1.0 m above seabed, as recorded during the September 5 storm event, represents the threshold for movement of 0.4 mm sand under unidirectional flow (MILLER et al., 1977). As bottom sediment across the upper shoreface consists mainly of medium to fine sand (0.2-0.35 mm), sediment transport would be limited only by the duration of the currents and these were observed to continue for up to 36 hours. The presence of shore-normal sand patches incised into megaripple field is strong evidence for this offshore transport of sand. It is likely that a proportion of the sand would be transferred to the lower shoreface and inner shelf zones below fair-weather wave base, and would not be returned by the action of fair-weather wave orbital currents. This would result in a long term net offshore transport of sand. HEQUETTE and HILL (1989) have noted the development of a Holocene transgressive sand sheet on the inner shelf of the Tuktoyaktuk Peninsula.

CONCLUSIONS

1. Several significant storms from the northwest in late August and early September 1987 resulted in substantial wave activity in Tibjak Beach nearshore zone, leading to beach erosion.
2. Two distinct sediment transport patterns were identified: (i) longshore transport to the south, from wave approach just north of shore normal; and (ii) longshore transport to the north combined with seaward-directed current transport, from wave approach just south of shore normal.
3. The seaward-directed currents may be rip currents, bottom return flows following storm surge set-up, or a combination of both.
4. Shallow channels, truncating fields of shore-parallel megaripples in 4 m water depth, are interpreted to have formed from the seaward-directed currents.

5. The seaward-directed currents probably account for significant offshore sediment transport of sand, some of which is permanently transferred to the lower shoreface and inner shelf below fair-weather wave base, thus contributing to the production of the transgressive sand sheet that occurs on the inner shelf of the Tuktoyaktuk Peninsula.

ACKNOWLEDGEMENTS

We gratefully acknowledge the financial support of the project by the Geological Survey of Canada and the Northern Oil and Gas Action Program. Logistic support was provided by the Polar Continental Shelf Project. The current meters and video cameras were deployed by G. Pierlot and D. Tuele of Arctic Sciences Ltd (Dartmouth, N.S). The time-control camera system was designed by Lobsiger Associates (Halifax, N.S.). We thank P.W. Barnes, B. Chapman, E. Kempema and A. McLean for their help aboard the R/V Karluk, W. Prime and J. Shaw for their help with the wave refraction analysis and D. Fissel (Arctic Sciences Ltd) for helpful advice concerning the current meter data. The ideas developed in this paper benefited from discussions with D.L. Forbes and M.H. Ruz. Thanks to R.B.Taylor for the interest he showed in the project.

LITERATURE CITED

BALSILLIE, J.H. and CARTER, R.W.G., 1984. The visual estimation of shore-breaking wave heights. Coastal Engineering, 8, 367-385.

BLASCO, S.M., FORTIN, G., HILL, P.R., O'CONNOR, M.J. and BRIGHAM-GRETTE, J. (in press). The late Neogene and Quaternary stratigraphy of the Canadian Beaufort continental shelf. In: A. Grantz, L. Johnson and J.F. Sweeney (eds.), The Arctic Ocean Region, Geological Society of America, The Geology of North America, v. L., Boulder, Colorado.

BOWEN, A.J. and INMAN, D.L., 1969. Rip currents, 2: laboratory and field observations. Journal of Geophysical Research, 74, 5479-5490.

BRUNO, R.O., DEAN, R.G., and GABLE, C.G., 1980. Longshore transport evaluations at a detached breakwater. Proceedings of the 17th Conference on Coastal Engineering, American Society of Civil Engineers, 1-23.

COASTAL ENGINEERING RESEARCH CENTRE, 1977. Shore Protection Manual (3rd ed.), US Army Corps of Engineers, Fort Belvoir, Va.

COOK, D.O., 1970. The occurrence and geologic work of rip currents off southern California. Marine Geology, 9, 173-186.

FISSEL, D.B. and BYRNE, O.J., 1988. Current and directional wave measurements in the Beaufort Sea coastal zone, August - September 1987. Geological Survey of Canada Open File 2069, 44 p.

FORBES, D.L., 1980. Late-Quaternary sea levels in the southern Beaufort Sea. Geological Survey of Canada, Current Research, Paper 80-1B, 75-87.

GALVIN, C.J., 1972. Wave breaking in shallow water. In: R.W. Meyer (ed.), Waves on Beaches, Academic Press, New York, NY, pp. 413-456.

GILLIE, R.D., 1985. King Point coastal zone sediment transport study (Contractors Report on Field Operations). Dobrocky Seatech Ltd., Sidney, BC, for Atlantic Geoscience Centre, Geological

Survey of Canada, Dartmouth, NS, 30 p.

GUZA, R.T. and INMAN, D.L., 1975. Edge waves and beach cusps. Journal of Geophysical Research, 80, 2997-3012.

GUZA, R.T. and BOWEN, A.J., 1975. The resonant instabilities of long waves obliquely incident on a beach. Journal of Geophysical Research, 80, 5429-4534.

HARDISTY, J. and LAVER, A.J., 1989. Breaking waves on a macrotidal barred beach: A test of McCowan's criteria. Journal of Coastal Research, 5, 79-82.

HARPER, J.R. and PENLAND, S., 1982. Beaufort Sea Sediment Dynamics. Unpublished report by Woodward-Clyde Consultants, Victoria (BC) for Geological Survey of Canada, 125 pp.

HARPER, J.R., REIMER, P.D. and COLLINS, A.D., 1985. Canadian Beaufort Sea Physical Shore-Zone Analysis. Geological Survey of Canada Open File 1689, 105 pp.

HARPER, J.R., HENRY, R.F. and STEWART, G.G., 1988. Maximum storm surge elevations in the Tuktoyaktuk region of the Canadian Beaufort Sea. Arctic, 41, 48-52.

HEQUETTE, A. and HILL, P.R. 1989. Late Quaternary seismic stratigraphy of the inner shelf seaward of the Tuktoyaktuk Peninsula, Canadian Beaufort Sea. Canadian Journal of Earth Sciences, 26, 1990-2002.

HEQUETTE, A. and BARNES, P.W. 1990. Coastal retreat and shoreface profile variations in the Canadian Beaufort Sea. Marine Geology, 91, 113-132.

HEQUETTE, A. and RUZ, M.H. (in prep.). Spit and barrier island migration in the southeastern Canadian Beaufort Sea.

HILL, P.R., MUDIE, P.J., MORAN, K. and BLASCO, S.M., 1985. A sea-level curve for the Canadian Beaufort Shelf. Canadian Journal of Earth Sciences, 22, 1383-1393.

INMAN, D.L. and BAGNOLD, R.A., 1963. Beach and Nearshore Processes, Part II: Littotal Processes. In: M.N. Hill (ed.), The Sea: Ideas and Observations, Vol. 3, Interscience, New York, NY, pp. 529-553.

KAMPHUIS, J.W., DAVIES, M.H., NAIRN, R.B. and SAYAO, O.J., 1986. Calculation of littoral sand transport rate. Coastal Engineering, 10, 1-21.

KOMAR, P.D., 1976. Beach Processes and Sedimentation, Prentice-Hall, Englewood Cliffs, NJ, 429 p.

KOMAR, P.D. and INMAN.D.L., 1970. Longshore sand transport on beaches. Journal of Geophysical Research, 75 (30), 5514-5527.

LONGUET-HIGGINS, M.S., 1952. On the statistical distribution of the heights of sea waves. Journal of Marine Research, 11, 245-266.

MAY, J.P., 1974. WAVENRG: A computer program to determine the distribution of energy dissipation in shoaling water waves with examples from coastal Florida. In: W.F. Tanner (Ed.), Sediment Transport in the Nearshore Zone, Florida State University, Tallahassee, Fl., pp. 22-80.

McCOWAN, J. (1894): On the highest wave of permanent type. Philos. Mag. Edinburgh, 32, 351-358.

MILLER, M.C., McCAVE, I.N. and KOMAR, P.D., 1977. Threshold of sediment motion under unidirectional currents. Sedimentology, 24, 507-528.

MORANG, A. and McMASTER, R.L., 1980. Nearshore bedform patterns along Rhode Island from side-scan sonar surveys. Journal of Sedimentary Petrology, 50, 831-840.

NIEDORODA, A.W., SWIFT, D.J.P., HOPKINS, T.S. and MA, C.M., 1984. Shoreface morphodynamics on wave-dominated coasts. Marine Geology, 60, 331-354.

PINCHIN, B.M., NAIRN, R.B. and PHILPOTT, K.L., 1985. Beaufort Sea coastal sediment study: numerical estimation of sediment transport and nearshore profile adjustment at coastal sites in the Canadian Beaufort Sea. Geological Survey of Canada Open File 1259.

RAMPTON, V.N., 1988. Quaternary geology of the Tuktoyaktuk coastlands, Northwest Territories. Geological Survey of Canada Memoir 423, 98 pp.

REIMNITZ, E., TOIMIL, L.J., SHEPARD, F.P. and GUTIERREZ-ESTRADA, M., 1976. Possible

rip current origin for bottom ripple zones to 30 m depth. Geology, 4, 395-400.

REINECK, H.E. and SINGH, I.B, 1980. Depositional Sedimentary Environments (2nd edition). Springer-Verlag, Berlin.

SHEPARD, F.P., EMERY, K.O. and LAFOND, E.C., 1941. Rip currents: a process of geological importance. Journal of Geology, 49, 337-369.

SVERDRUP, H.U. and MUNK, W.H. (1946): Theoretical and empirical relations in forecasting breakers and surf. Trans. Am. Geophys. Union, 27, 828-836.

SWIFT, D.J.P., NIEDERODA, A.W., VINCENT, C.E. and HOPKINS, T.S., 1985. Barrier island evolution, middle Atlantic Shelf, U.S.A., Part I: shoreface dynamics. Marine Geology, 63, 331-361.

VILKS, G., WAGNER, F.J.E. and PELLETIER, B.R., 1979. The Holocene marine environment of the Beaufort Shelf. Geological Survey of Canada Bulletin 303, 43 pp.

WHITE, T.E. and INMAN, D.L., 1989. Measuring longshore transport with tracers, Ch. 13 in R.J. Seymour (ed), Nearshore Sediment Transport, Plenm, New York, 400 pp.

WRIGHT, L.D., CHAPPELL, J., THOM, B.G., BRADSHAW, M.P. and COWELL, P., 1979. Morphodynamics of reflective and dissipative beach and inshore systems: southeastern Australia. Marine Geology, 32, 105-140.

WRIGHT, L.D. and SHORT, A.D., 1984. Morphodynamic variability of surf zones and beaches: a synthesis. Marine Geology, 56, 93-118.

LIST OF SYMBOLS

a	Wave amplitude (m) = H/2
a'	Pore-space factor for immersed weight of sand (≈ 0.6 for well sorted sand)
b	(subscript); denotes breaking wave conditions
C	Wave phase velocity (m s^{-1})
D	Sediment size (m)
d	Water depth (m)
g	Acceleration of gravity (= 9.8 m s^{-2})
H	Wave height (m)
I_l	Immersed weight longshore sediment transport rate (N s^{-1})
K	Constant in CERC formula
n	Ratio of group velocity to phase velocity
P_l	Longshore component of wave power (W m^{-1})
Q_l	Volumetric longshore sediment transport rate (m^3 s^{-1})
Q'_l	Dry mass longshore sediment transport rate (kg s^{-1})
s	(subscript); related to significant wave unless otherwise defined
T	Wave period (s)
α_b	Wave angle with shoreline at breaking
ß	Beach/surf zone slope (°) = d_b/λ
γ	Breaker index = H_b/d_b (≈ 0.78)
λ	Distance from still water line to breakpoint (m)

ε Surf-scaling parameter

ρ Mass density of sea water (= 1.02 X 10^3 kg m^{-3})

ρ_s Mass density of sediment (= 2.65 X 10^3 kg m^{-3} for quartz sand)

ω Wave radian frequency (= $2\pi/T$)